Research article

Research for the spall effect after ballistic impact with finite element method

Volkan Arıkan[a], Bulut Berk[a], Ramazan Karakuzu[a], A. Kaan Toksoy[b], Onur Sayman[c]*

[a]*Mechanical Engineering Department, Engineering Faculty, Dokuz Eylül University, Turkey*
[b]*Roketsan A.Ş., Turkey*
[c]*Mechanical Engineering Department, Engineering Faculty, Gediz University, Turkey*

Abstract

In this study, the fragmentation occurring with ballistic impact was researched with finite element method by using Ansys Autodyn software, and using different modelling methods, the most accurate and precise method was selected for the problem. After determining the method, the finite element model was generated and solved for two different types of ballistic armor (Al5083 & RHA). Spall distribution was observed and close results obtained between finite element and experimental study. Having good agreement between experimental and numerical study the research continued with spall liner (Kevlar/epoxy) addition after armor plate to reduce spall distribution.

©2014 Usak University all rights reserved.

1. Introduction

The damage of a high velocity projectile impact on an armor plate is not just perforation. In some cases, whether the plate punctured or not, there might be spallation occurs on the rear side of the plate. As a result of this spallation so many particles having different shapes and velocities are scattered through the environment. This causes serious damage and injuries. A study, that interested to block this spallation or reduce its effects, should focus on to specify the spalling particles properties first. These kind of experimental studies have high cost due to computer aided modelling and analysis has more importance. There are different discrimination methods (Lagrange, Euler, and Arbitrary Lagrangian Eulerian) and mesh-free methods for studying this kind of numeric analysis. Başaran [1] studied bird strike simulations and he proposed a mesh free method SPH (smooth particle hydrodynamics) has an advantage of solution time, precision, and showing large deformations and spall more accurate than other methods. Huang *et al.* [2] proposed a new debris cloud model based on statistical principles to obtain the detail of debris cloud. They used SPH method for the analyses and they had close results between experimental and numerical studies, but for the identification of the SPH particles they

developed a program called DebrisID. Loft *et al.* [3] studied high velocity impact tests varying 1–8.5 km/s experimentally and numerically with using SPH method in Ansys Autodyn software. They had close results within 10%. Hayhurst and Cleeg [4] studied SPH method; they investigated debris cloud and particle velocities after ballistic impact experimentally and numerically. They had close results between experimental and numerical studies. Lee [5] investigated penetration depth and ballistic limit velocity of ceramic/metal composites after high velocity impact using mesh free SPH method.

In this study, the spallation which occurs after ballistic impact was investigated experimentally and numerically using Ansys Autodyn software. The mesh free SPH method was used because of some advantages like offering precise results for large deformations and spalling, solution time. This numerical method and experimental work were tested for two types of armor (Al5083 and RHA), spall angle and velocities. Close results were obtained between experimental and numerical studies. Obtaining close results, numerical studies continued with addition of composite spall liner to model and its effect on spall was investigated.

2. Material and Method

2.1. Ballistic Tests

The test fixture was manufactured properly for the specified standards. Test fixture is shown in Fig. 1. In these tests HEAT ammunition was used and detonated. After each test, the damage, which occurs on plate and the witness plate was measured. There are different types of armor structures used in this kind of tests. In this study, RHA and Al5083 alloy was used. The witness plate pack was placed 600 away under the armor plate. The witness plates were arranged as mentioned by ITOP (International Test Operations Procedure). Witness plate arrangement is shown in Fig. 2.

Fig. 1 Test fixture

Al (3x1 mm)

Al (1 mm)

Steel (1.5 mm)

25 mm thickness foam
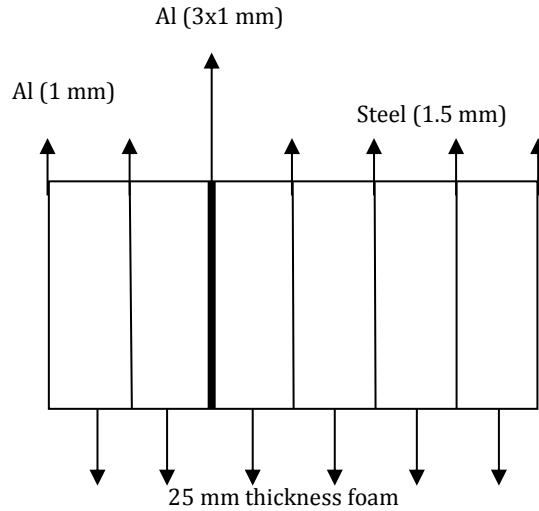
Fig. 2 Witness plate arrangement

2.2. Numerical Analysis

Numerical analysis was studied with Ansys Autodyn software. The warhead was modelled with lagrangian while plates and composite structures were modelled with SPH (Smooth Particle Hydrodynamics) method. Material models were taken from material library in Autodyn software [6]. The mechanical properties of the used materials are shown in Table 1-4.

Table 1
Mechanical properties of copper

	EOS – Shock			
Gruneisen Coefficient	C1 (m/s)	S1	Ref. Temperature (K)	Specific Heat (J/kgK)
2.02	3940	1.489	300	383

	Strength (Steinberg Guinan)			
Shear Modulus (GPa)	Yield Stress (MPa)	Hardening Constant	Hardening Exponent	Melting Temperature (K)
47.7	120	36	0.45	1790

Table 2
Mechanical properties of RHA

	EOS – Shock	
Gruneisen Coefficient	C1 (m/s)	S1
1.67	4610	1.73

Strength (von Mises)	
Shear Modulus (GPa)	Yield Stress (MPa)
64.1	1500

Table 3

Mechanical properties of Al5083

EOS – Linear			
Bulk Modulus	Ref.Temperature (K)	Specific Heat (J/kgK)	
2.02	293	910	

Strength Properties (Johnson Cook)				
Shear Modulus (GPa)	Yield stress (MPa)	Hardening Constant (MPa)	Hardening Exponent	Melting Temperature (K)
26.92	167	596	0.551	893

Table 4

Mechanical properties of Kevlar/Epoxy

EOS - Orthotropic						
E_{11} (GPa)	E_{22} (GPa)	E_{33} (GPa)	v_{12}	v_{23}	v_{31}	S_{12} (GPa)
3,248	13	13	0.0775	0.0625	0.312	1

Failure Properties		
Tensile Failure Strain 11	Tensile Failure Strain 22	Tensile Failure Strain 33
0.01	0.08	0.08

Tests were modelled in 2D, and material model was chosen with respect to this condition. In composite modelling '1' shows material thickness direction, '2' shows fiber direction and '3' shows the perpendicular direction to a fiber. Boundary conditions are set as the tests. Virtual gauges were placed on the rear side of the armor at 5 mm intervals for determining the spallation properties. The boundary conditions and gauge settling are shown in Fig. 3.
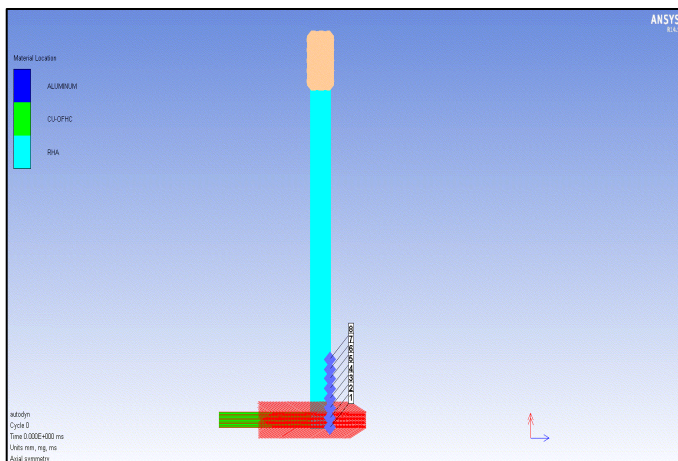
Fig. 3 Boundary conditions and gauge settling

3. Results and Discussion

3.1. Test Results

3.1.1. RHA Tests

RHA armor dimensions were chosen as 400x400x12.7 mm^3. The deformation after the test is shown in Fig. 4.
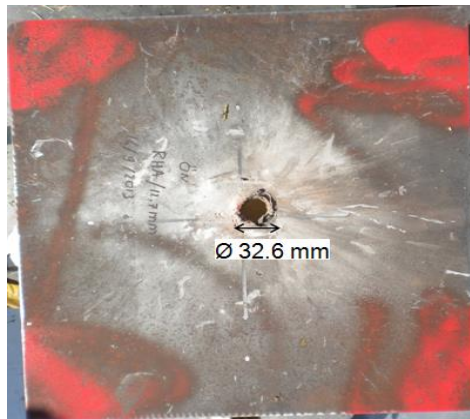

Fig. 4 Deformation of the RHA armor plate

After the test, the distribution of the spall was measured and spallation diameter was observed as 900 mm. Spall effect on the witness plate is shown in Fig. 5.

**Fig. 5** Spall effect on the witness plate

3.1.2. Al5083 Tests

Al5083 alloy plate dimension was chosen as 400x400x38 mm^3. This armor plate had more deformation than the RHA plate. The deformation that occurs in front and the rear side of the plate is shown in Fig. 6.

Fig. 6 Deformation of the Al5083 armor plate

After this test the spallation diameter was observed at 1300 mm. In this test, spallation diameter and spalling particles dimensions increased dramatically. Spall effect after the test is shown in Fig. 7.
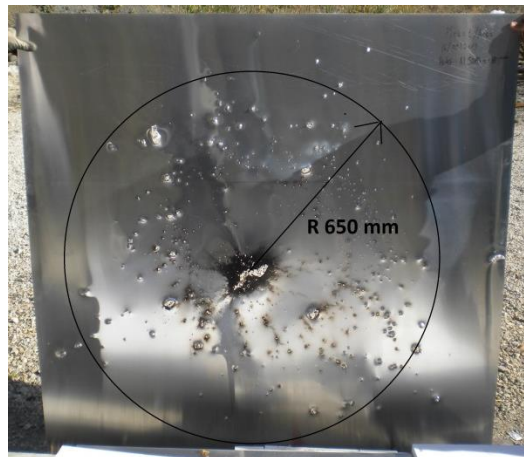

Fig. 7 Spall effect after impact

3.2. Numeric Analysis Results

3.2.1. RHA Tests

The deformation and spall distribution of RHA plate after numeric analysis is shown in Fig. 8. The perforation diameter of the armor plate was measured as 41 mm in diameter and spallation diameter was measured 820 mm. The spall particles have different velocities with respect to distance from jetting center. Some examples of these velocities are shown in Fig. 9.
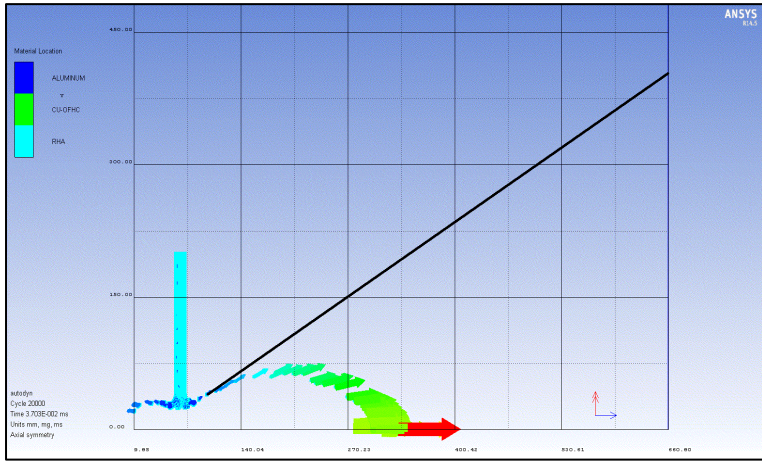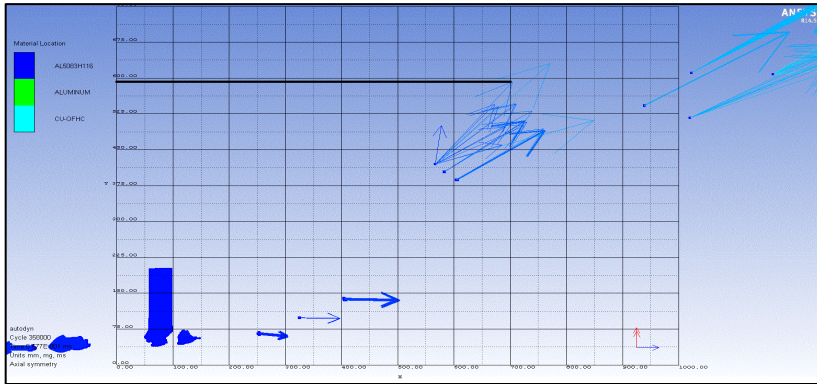
Fig. 8 Spall distribution of the RHA plate
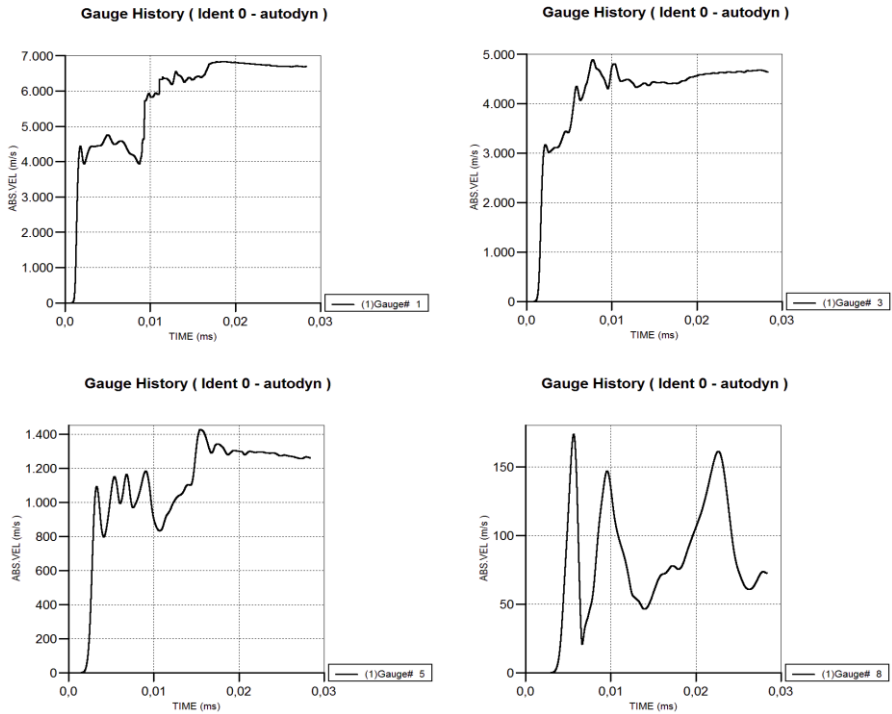
Fig. 9 Gauge by gauge particle velocities

3.2.2. Al5083 Tests

In this analysis, the same procedure was applied to Al5083. The deformation and spallation is shown in Fig. 10. The perforation of the plate was measured as 74 and 120 mm for the front and the rear side of armor. Spallation diameter was measured at 1200 mm.

Fig. 10 Spall distribution of the Al5083 plate

In comparisons between numerical and experimental results, we find the spallation diameters are in good agreement, at the same time the deformation of the plate isn't as well as spallation data. But they both have close results.

3.2.3. RHA & Composite Liner

In this analysis, kevlar/epoxy composite plate was settled in the model and the spall liner effect on spallation was examined. The model and the boundary conditions are shown in Fig. 11.
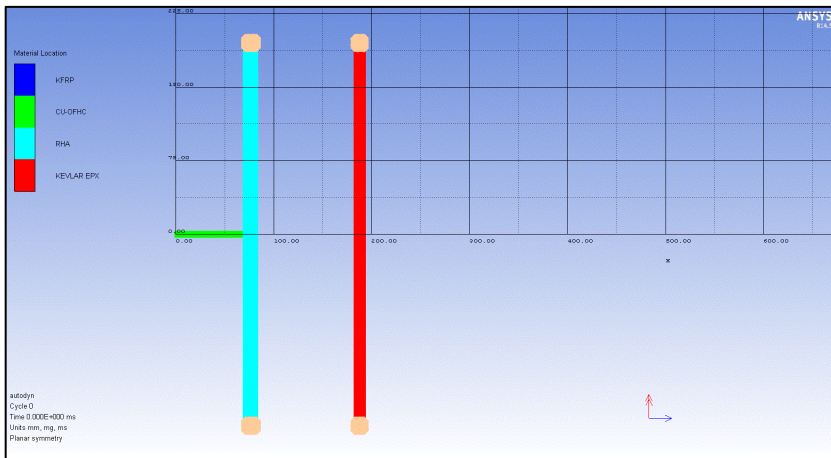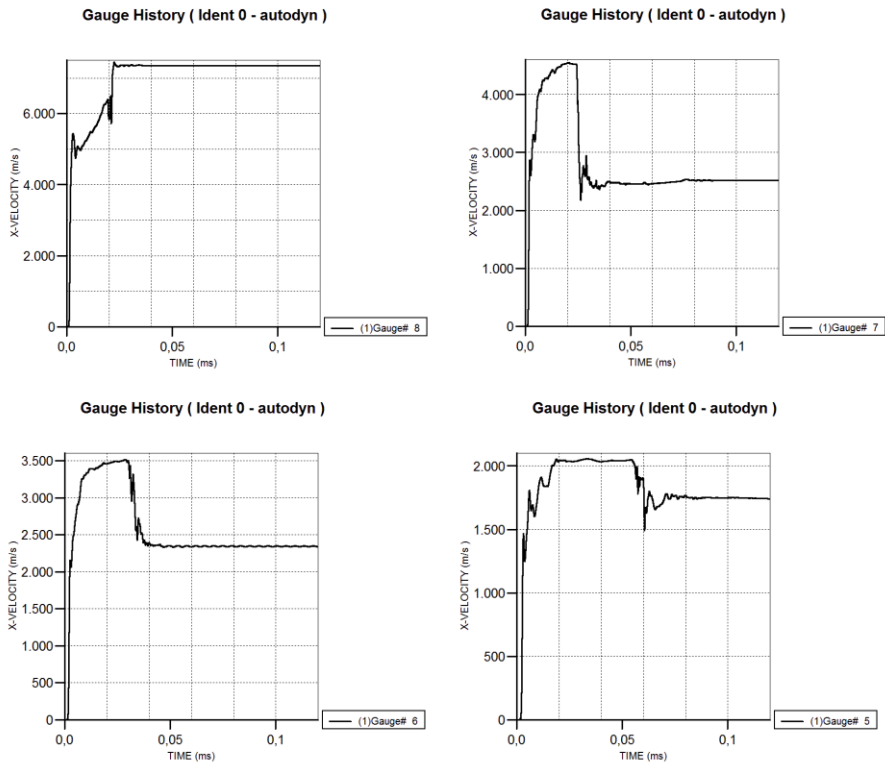

Fig. 11 Numerical model and boundary conditions

Spallation diameter was measured 700 mm after solution. Debris cloud after impact and velocities of the spalling particles are shown in Figs. 12 and 13.
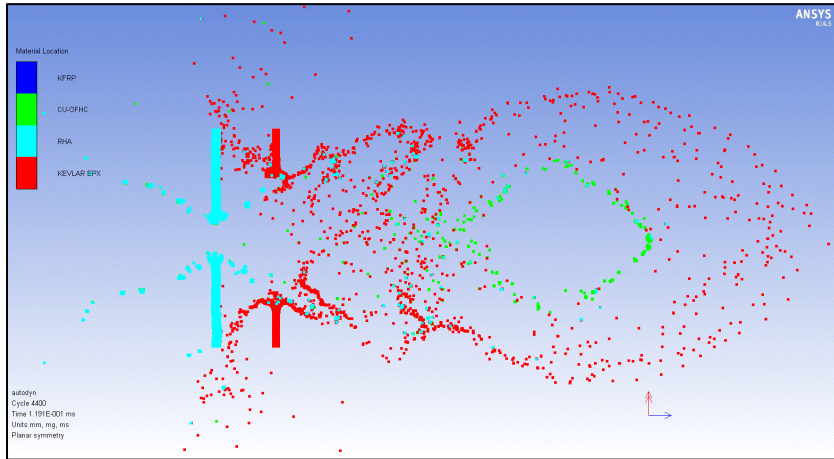
Fig. 12 Debris cloud after impact

Fig. 13 Gauge by gauge particle velocities

In composite modelling, mesh free methods were chosen because of their effectiveness on showing delamination, failure, and the boundary after deformation. Comparison between the particle velocities that observed from different (with/without spall liner) numeric analysis, we can easily say that spall liner reduced the particle velocities significantly. Also the liner addition helps to reduce spallation angle, but on the other hand the spall intensity increased as seen in the debris cloud in fig.12. To reduce the

particle velocities and spallation diameter, the research will continue with changing the spall liner properties and placing.

Finally, the numerical and experimental studies showed that ballistic impact and its effects determined well in numerical analysis. This means low experimental costs and solution time, especially in design process.

Acknowledgement

References

1. Başaran G. Bird strike analysis. Figes Article, Research&Development Journal, 2013; 1: 8 – 10.
2. Huang J, Ma Z, Ren L, Li Y, Zhou Z, and Liu S. A new engineering model of debris cloud produced by hypervelocity impact. International Journal of Impact Engineering, 2013; 56: 32 – 39.
3. Loft K, Price MC, Cole MJ, and Burchell MJ. Impacts into metal targets at velocities greater than 1 km s^{-1}: A new online resource for the hypervelocity impact community and illustration of the geometric change of debris cloud impact patterns with impact velocity. International Journal of Impact Engineering, 2013; 56: 47 – 60.
4. Hayhurst CJ and Clegg RA. Cylindrically symmetric SPH simulations of hypervelocity impacts on thin plates. International Journal of Impact Engineering, 1997; 20: 337 – 348.
5. Lee M. Hypervelocity impact into oblique ceramic/metal composite systems. International Journal of Impact Engineering, 2003; 29: 417 – 424.
6. ANSYS® Academic Research, Release 14.0, Autodyn, Material library, ANSYS, Inc.